

Nonadiabatic dynamics of electron scattering from adsorbates in surface bandsBranko Gumhalter,¹ Antonio Šiber,¹ Hrvoje Buljan,² and Thomas Fauster³¹*Institute of Physics, HR-10000 Zagreb, Croatia*²*Department of Physics, University of Zagreb, HR-10002 Zagreb, Croatia*³*Lehrstuhl für Festkörperphysik, Universität Erlangen-Nürnberg, D-91058 Erlangen, Germany*

(Received 5 June 2008; published 9 October 2008)

We present a comparative study of nonadiabatic dynamics of electron scattering in quasi-two-dimensional surface band which is induced by the long-range component of the interactions with a random array of adsorbates. Using three complementary model descriptions of intraband spatiotemporal propagation of quasiparticles that go beyond the single-adsorbate scattering approach we are able to identify distinct subsequent regimes of evolution of an electron following its promotion into an unoccupied band state: (i) early quadratic or ballistic decay of the initial-state survival probability within the Heisenberg uncertainty window, (ii) preasymptotic exponential decay governed by the self-consistent Fermi golden rule scattering rate, and (iii) asymptotic decay described by a combined inverse power-law and logarithmic behavior. The developed models are applied to discuss the dynamics of intraband adsorbate-induced scattering of hot electrons excited into the $n=1$ image-potential band on Cu(100) surface during the first stage of a two-photon photoemission process. Estimates of crossovers between the distinct evolution regimes enable assessments of the lifespan of a standard quasiparticle behavior and thereby of the range of applicability of the widely used Fermi golden rule and optical Bloch equations approach for description of adsorbate-induced quasiparticle decay and dephasing in ultrafast experiments.

DOI: [10.1103/PhysRevB.78.155410](https://doi.org/10.1103/PhysRevB.78.155410)

PACS number(s): 73.20.-r, 79.60.-i, 71.10.-w, 78.47.J-

I. INTRODUCTION

Recent developments in the applications of ultrafast photoelectron spectroscopy have enabled studies of electron dynamics at surfaces in the real time domain. This provided novel insights into the temporal evolution and decoherence of surface-localized electronic states and opened up new directions in the investigations of surface interactions and reactions on the ultrashort time scale. In this context the electronic states within the quasi-two-dimensional Shockley surface state (SS) and image-potential state (IS) bands on low-index crystal surfaces of fcc and bcc metals have served as paradigms in the studies of dynamics of quasiparticles at surfaces and their interactions with the environment.

Many important aspects of hot electron energetics and dynamics in surface-localized bands have been successfully explored in two-photon-photoemission (2PPE) experiments by combining the use of continuous wave as well as pulsed pump and probe laser beams with variable delay times. This has resulted in accumulation and systematization of the data on characteristic energies and lifetimes of hot electron and hole excitations in Shockley and image-potential bands on clean surfaces¹⁻¹³ and surfaces covered with localized defects¹⁴⁻¹⁹ (adsorbates, cavities, steps, etc.). Various theoretical approaches have been employed to interpret the measured energy levels and linewidths of surface and image-potential states within the microscopic models. Band-structure calculations have provided underlying framework for the understanding of one-electron dynamics at ideal surfaces.²⁰⁻²² This laid foundation for the studies of spectral linewidths of surface-localized states that arise from dynamical interactions with the environment, i.e., with the various degrees of freedom of the system, and the obtained results have been used in the development of microscopic theories

of 2PPE from surfaces.²³⁻²⁶ In the next step the investigations have been extended to quasiparticle scattering from surface defects which is a prerequisite for the understanding of fundamental processes in more complex structures. Calculations of electron and hole decay and dephasing rates that arise from elastic scattering from single adsorbates have demonstrated the important contribution of this scattering mechanism to the overall linewidths of electronic states in surface bands even for small adsorbate concentrations.²⁷⁻³³

The majority of treatments of the dynamics of quasiparticles excited into surface bands during the first stage of a 2PPE event have been restricted to the adiabatic or Markovian (quasistationary) picture. In this approximation the temporal evolution of quasiparticle states is characterized by exponential decay governed by the Fermi golden rule (FGR) type of transition rates. Such a description is applicable to a steady state evolution of the system during the times that are on the order of or exceed the relaxation times typical of the system. This regime was tacitly assumed in the developments of first microscopic theories of 2PPE from surface²³⁻²⁶ and bulk³⁴ bands. The applicability of phenomenological optical Bloch equations in the simulations of time-resolved 2PPE experiments^{7,13,26,35-37} also rests on this assumption. However, 2PPE measurements utilizing pump and probe laser pulses of femtosecond duration and small delay times also probe the early non-Markovian evolution of quasiparticles excited in surface bands. Besides the possible direct consequences on the measured 2PPE spectra, this fact may turn out important in the determination of 2PPE correlation traces since in that case the delay times are varied from negative to positive values across zero, in which case the non-Markovian and Markovian evolution of excited quasiparticles may equally contribute to the results of measurements.

First investigations of the problem of decay and decoherence of quasiparticles promoted into Shockley and image-

potential bands on clean metal surfaces that go beyond the Markovian approximation were reported in Refs. 38 and 39 utilizing concepts and methods developed earlier.^{40–44} Here the decay processes were assumed to arise from quasiparticle interactions with electronic charge density fluctuations in the system. The calculated quasiparticle survival probabilities presented in Refs. 38 and 39 demonstrate that within the first 10 fs following the electron and hole excitation in the IS and SS band, respectively, their evolution markedly deviates from the Markovian exponential decay governed by the FGR decay rate. Only past that interval the evolution of quasiparticles can be described by a *modified* or self-consistent FGR-governed exponential decay.

In the present work we extend these investigations to the problem of multiple IS-electron scattering induced by the interactions with low concentrations of adsorbed atoms randomly distributed over the surface. This problem has been extensively studied experimentally and many of its aspects also theoretically. Angle- and time-resolved 2PPE spectroscopy measurements have shown that the decoherence and decay effects arising from excited electron scattering by small concentration of random defects can be as large as those originating from the interactions with charge density fluctuations in the system.¹⁸ Recent developments in time-resolved interferometric photoemission technique^{10,45} make possible the separation of dephasing processes originating from inelastic electron scattering and quasielastic scattering by impurities. Theoretical studies of IS-electron scattering from *single* adsorbates have demonstrated that intraband transitions responsible for dephasing are caused dominantly by the long-range component of the electron-adsorbate potential which gives rise to small momentum transfer in elastic scattering.^{17,31} Our investigations focus on the elucidation of dynamics of intraband electron scattering by dipolar potentials of random adatoms and its dependence on the concentration of scatterers.

2PPE spectra from quasi-two-dimensional surface bands provide information on the dynamics of electronic states described by the quasiparticle momentum \mathbf{K} parallel to the surface and the band index n , which are good quantum numbers for the description of unperturbed quasiparticle motion in surface bands. To study the temporal aspects of photoexcited electron scattering from arrays of adsorbates we shall calculate the quasiparticle survival probability which describes electron evolution after its promotion into an eigenstate in the band. Physical reasons for the choice of unperturbed states as initial quasiparticle states in the treatment of relaxation processes are explained in Ref. 46. Thus, we start from the *unperturbed* electron wave function $\Psi_{\mathbf{K},n}^0(0)$ in a band state $|\mathbf{K},n\rangle$ at the instant $t=0$ and investigate how it develops in the course of time due to intraband scattering. We first define the propagation amplitude whose magnitude and phase carry the relevant information on quasiparticle evolution in the course of time by the expression

$$A_{\mathbf{K},n}(t) = \langle \Psi_{\mathbf{K},n}^0(0) | \Psi_{\mathbf{K},n}(t) \rangle, \quad (1)$$

where $\Psi_{\mathbf{K},n}(t)$ is the electron wave function that evolved from unperturbed $\Psi_{\mathbf{K},n}^0(0)$ in the presence of interaction with

adsorbates. The quasiparticle survival probability in the interval $(0,t)$ is then obtained as

$$L_{\mathbf{K},n}(t) = |A_{\mathbf{K},n}(t)|^2 \quad (2)$$

and the quasiparticle phase as

$$\phi_{\mathbf{K},n}(t) = -\text{Im} \ln[A_{\mathbf{K},n}(t)]. \quad (3)$$

The quasiparticle amplitude (1), and hence $L_{\mathbf{K},n}(t)$ and $\phi_{\mathbf{K},n}(t)$, can be calculated within several different approaches to the scattering problem. In the following sections we shall employ three complementary methods for their calculation and combine them to establish a global picture of the dynamics of IS-electron scattering from low density of random adsorbates.

II. CALCULATION OF THE QUASIPARTICLE SURVIVAL PROBABILITY IN THE SELF-ENERGY APPROACH

The quantum-mechanical problem of electron scattering by a random array of impurities in solids has a long history and has been addressed within several different formalisms. A good physical insight into the various stages of dynamics of electrons excited into an empty surface band, where their propagation becomes affected by the interactions with localized scatterers, can be obtained in the Green's function or spectral approach to the calculation of propagation amplitudes and survival probabilities. This formalism enables a direct contact with the results of earlier treatments of the decay and dephasing of electronic states in surface bands based on the Fermi golden rule approach and also provides a suitable framework for discussions of the results obtained by complementary methods described in Secs. III and IV.

In this section we present a calculation of the scattered IS-electron Green's function in the self-energy approach. The development and use of this formalism is explained in detail in Ref. 47. In the present problem it is assumed that the electron is initially injected⁴⁸ (i.e., excited or pumped by photon absorption at an instant within the pump pulse duration) into an unperturbed momentum eigenstate $|\mathbf{K},n=IS\rangle$ in the unoccupied IS band from which it evolves into a state perturbed by the interaction with adsorbates. Introducing the creation and annihilation operators $c_{\mathbf{K},n}^\dagger$ and $c_{\mathbf{K},n}$, respectively, for electron states characterized by quantum numbers \mathbf{K} and n , we may express the wave functions appearing in Eq. (1) as

$$|\Psi_{\mathbf{K},n}^0(0)\rangle = c_{\mathbf{K},n}^\dagger |0\rangle, \quad (4)$$

and

$$|\Psi_{\mathbf{K},n}(t)\rangle = \exp(-iHt)c_{\mathbf{K},n}^\dagger |0\rangle, \quad (5)$$

where $|0\rangle$ denotes empty IS band and $\exp(-iHt)$ is the evolution operator (we use atomic units in which $\hbar=1$) in which H is the one-electron Hamiltonian describing electron motion in the IS band in the presence of interactions with adsorbates. This enables to represent propagation amplitude (1) in terms of the retarded single-electron Green's function $G_{\mathbf{K},n}(t)$ as

$$A_{\mathbf{K},n}(t) = \langle 0 | c_{\mathbf{K},n} \exp(-iHt) c_{\mathbf{K},n}^\dagger | 0 \rangle \Theta(t) = iG_{\mathbf{K},n}(t). \quad (6)$$

The Hamiltonian H is represented as a sum of the unperturbed part and the interaction with adsorbates

$$H = H_0 + V. \quad (7)$$

The unperturbed part is expressed as

$$H_0 = \sum_{\mathbf{K}} E_{\mathbf{K},\text{IS}} c_{\mathbf{K},\text{IS}}^\dagger c_{\mathbf{K},\text{IS}}, \quad (8)$$

where $E_{\mathbf{K},\text{IS}}$ denote the unperturbed one-electron energies in the IS band. The interaction part that describes electron scattering from adsorbates is given by

$$V = \sum_{\mathbf{K}',\mathbf{K}} V_{\text{IS}}(\mathbf{K}' - \mathbf{K}) \rho(\mathbf{K}' - \mathbf{K}) c_{\mathbf{K}',\text{IS}}^\dagger c_{\mathbf{K},\text{IS}}. \quad (9)$$

Here $V_{\text{IS}}(\mathbf{K}' - \mathbf{K}) = \langle \mathbf{K}', \text{IS} | V(\mathbf{R} - \mathbf{R}_j, z - z_j) | \mathbf{K}, \text{IS} \rangle$ is the intraband matrix element of the *single-adsorbate potential* $V(\mathbf{R} - \mathbf{R}_j, z - z_j)$ centered at (\mathbf{R}_j, z_j) , and

$$\rho(\mathbf{K}' - \mathbf{K}) = \sum_j e^{-i(\mathbf{K}' - \mathbf{K})\mathbf{R}_j} \quad (10)$$

is the two-dimensional Fourier transform (2D FT) of the density $\sum_j \delta(\mathbf{R} - \mathbf{R}_j)$ of adsorbates (scattering centers) randomly distributed over the surface. In all expressions the symbols $\mathbf{R} = (x, y)$ denote radius vectors parallel to the surface and z is the coordinate perpendicular to the surface plane. In the following we omit the band indices IS as we consider only intraband scattering processes.

The retarded Green's function $G_{\mathbf{K}}(t)$ is calculated from its spectral representation

$$G_{\mathbf{K}}(t) = -i\Theta(t) \int_{-\infty}^{\infty} d\omega e^{-i\omega t} S_{\mathbf{K}}(\omega), \quad (11)$$

where the spectrum $S_{\mathbf{K}}(\omega)$ is expressed in terms of the quasiparticle self-energy arising from the interaction with adsorbates. For the self-energy represented as the sum of real and imaginary parts in the form $\Sigma_{\mathbf{K}}(\omega) = \Lambda_{\mathbf{K}}(\omega) - i\Gamma_{\mathbf{K}}(\omega)$, the spectrum is given as

$$S_{\mathbf{K}}(\omega) = \frac{1}{\pi} \frac{\Gamma_{\mathbf{K}}(\omega)}{[\omega - E_{\mathbf{K}} - \Lambda_{\mathbf{K}}(\omega)]^2 + \Gamma_{\mathbf{K}}(\omega)^2}, \quad (12)$$

and satisfies the normalization condition $\int_{-\infty}^{\infty} d\omega S_{\mathbf{K}}(\omega) = 1$. This approach to obtaining $G_{\mathbf{K}}(t)$ has several numerical and analytical advantages because it can make use of the calculation of Green's functions in the energy representation in which various contributions to the self-energy can be conveniently discerned and analyzed.⁴⁹

Calculation of the electron self-energy for the case of interactions with a *random array of scattering centers* is based on the ensemble averaging of the Green's function $G_{\mathbf{K}}(\omega)$

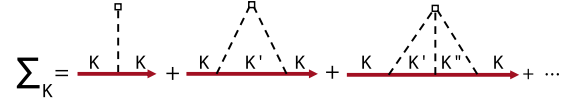


FIG. 1. (Color online) Lowest-order self-energy diagrams which are linear in the concentration of adsorbates. The full lines symbolize electron propagators and dashed lines the adsorbate scattering potential centered at the same site (denoted by small vertex quadrangle).

over random positions \mathbf{R}_j of the scatterers.⁴⁷ This amounts to averaging the various products of functions (10) appearing in the Dyson expansion of $G_{\mathbf{K}}(\omega)$. Such a procedure generates an expansion of the electron self-energy in powers of the concentration of adsorbates on the surface

$$c = n_{\text{ad}}/L^2, \quad (13)$$

where n_{ad} is the total number of adsorbates and L^2 is the surface area. For low concentrations c one may retain only the linear terms and obtain the expansion of the self-energy in powers of V_{IS} whose lowest-order Feynman diagrams are shown in Fig. 1 (the validity of this approximation will be further discussed and substantiated in Secs. III and IV). It should be noted that in each diagram of this expansion the dashed lines symbolizing the interaction potentials are all joined in a single vertex, which denotes repeated electron scattering from the same adsorbate. In each such process the total momentum transfer is zero. Scattering contributions from different adsorbates add incoherently and give rise to self-energy terms proportional to higher powers of concentration (13).⁴⁷

The leftmost diagram depicted in Fig. 1 describes the lowest-order forward scattering of electrons by adsorbates and gives a purely real contribution to the electron self-energy. As such, it can only contribute to a rigid shift or \mathbf{K} -independent renormalization of the energies of electron band states but not to their dephasing. In the following we shall assume that this static energy shift has been incorporated into the renormalized values of $E_{\mathbf{K}}$ and focus on the dynamical aspects of the problem described by higher-order terms in the expansion of quasiparticle self-energy.

If the scattering potentials are weak the leading contribution to the dephasing processes is described by the imaginary part of the middle diagram in Fig. 1. The approximation in which the self-energy expansion is terminated after the second term depicted in Fig. 1 is equivalent to calculating the electron scattering rate within the FGR approach. For intraband electron scattering by the dipolar potential of adsorbates discussed in Ref. 17 such an approximation seems to be well justified (see below) and we shall pursue it in this section. In this case we obtain for the imaginary part of the self-energy

$$\Gamma_{\mathbf{K}}(\omega) = n_{\text{ad}} \pi \sum_{\mathbf{K}'} |V_{\text{IS}}(\mathbf{K} - \mathbf{K}')|^2 \delta(\omega - E_{\mathbf{K}'}), \quad (14)$$

in which the substitution $n_{\text{ad}} = cL^2$ yields an expression proportional to c and free from the box normalization factor L^2 that enters through $V_{\text{IS}}(\mathbf{K}' - \mathbf{K}) \propto L^{-2}$ and

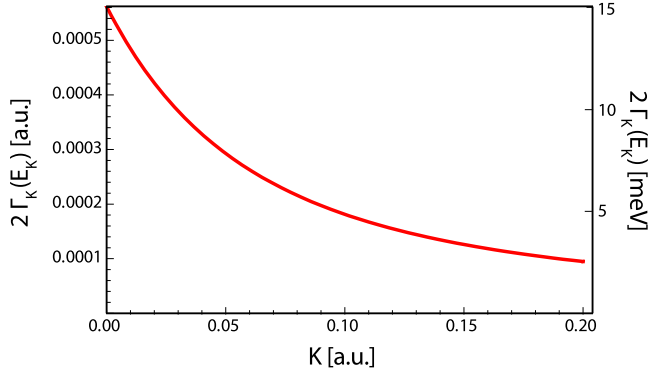


FIG. 2. (Color online) Excited IS-electron scattering or decay rate calculated from Fermi's golden rule expression (16) for the long-range dipole electron-adsorbate interaction taken from Ref. 17 and $\Theta=0.7\%$. Energy scale in a.u. (left) and meV (right).

$\Sigma_{\mathbf{K}'} \rightarrow L^2/(2\pi)^2 \int d^2\mathbf{K}'$. The real part of the self-energy is obtained from the Hilbert transform

$$\Lambda_{\mathbf{K}}(\omega) = \frac{1}{\pi} \int_{-\infty}^{\infty} d\omega' \frac{\Gamma_{\mathbf{K}}(\omega')}{\omega - \omega'}, \quad (15)$$

where the integral is the Cauchy principal value. The on-the-energy-shell constrained expression

$$2\Gamma_{\mathbf{K}}(E_{\mathbf{K}}) = n_{\text{ad}} 2\pi \sum_{\mathbf{K}'} |V_{\text{IS}}(\mathbf{K} - \mathbf{K}')|^2 \delta(E_{\mathbf{K}} - E_{\mathbf{K}'}) \quad (16)$$

gives the *bare* FGR result for the scattering (decay) rate or inverse lifetime $1/\tau_{\mathbf{K}}^{\text{FGR}}$ of the electron promoted into the initial state with momentum \mathbf{K} and energy $E_{\mathbf{K}}$. The total cross section for electron scattering from adsorbates per single adsorbate is then given by¹⁷

$$\sigma_{\mathbf{K}} = \frac{2\Gamma_{\mathbf{K}}(E_{\mathbf{K}})}{c j_{\mathbf{K}}}, \quad (17)$$

where $j_{\mathbf{K}} = K/m_e$ is the electron current in the state $|\mathbf{K}\rangle$.

Expression (17) was employed in Ref. 17 to calculate the cross section for IS-electron scattering from Cu adsorbates on Cu(100) surface starting from the assumption that long-range dipolar potential of adatoms favors small-momentum-transfer scattering events and thus dominantly determines elastic intraband transitions responsible for dephasing.⁵⁰ The validity of this approach was tested by comparing the cross sections obtained from expressions (14) and (17) and the ones measured in time-resolved 2PPE experiments.¹⁷ In the present calculation of the electron self-energy based on expressions (14) and (15) we shall adopt the model dipolar potential and electron wave functions from Ref. 17 in order to facilitate comparison and discussion of the dynamics of electron scattering reported in that work. For Cu(100) surface covered with Cu adatoms n_{ad} can be expressed in terms of the relative coverage Θ as $n_{\text{ad}} = \Theta L^2/d_{\text{nn}}^2$ yielding $c = \Theta/d_{\text{nn}}^2$ where d_{nn} is the nearest-neighbor distance between two Cu atoms in the (100) crystal plane. This enables the calculation of the FGR scattering rate (16) that is plotted in Fig. 2 for $\Theta=0.7\%$.

Figures 3 and 4 show the functions $\Gamma_{\mathbf{K}}(\omega)$, $\Lambda_{\mathbf{K}}(\omega)$, and

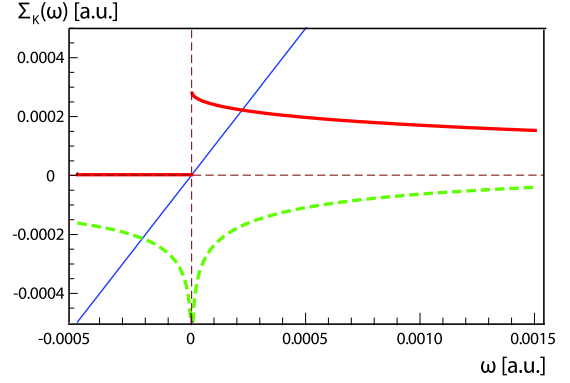


FIG. 3. (Color online) Plots of the imaginary part $\Gamma_{\mathbf{K}}(\omega)$ (full thick curve) and real part $\Lambda_{\mathbf{K}}(\omega)$ (dashed thick curve) of the self-energy $\Sigma_{\mathbf{K}}(\omega)$ for initial wave vector $K=0$. All energies are measured from the IS-band bottom $\omega=0$. The intersection of $\Lambda_{\mathbf{K}}(\omega)$ with the thin line $\omega - E_{\mathbf{K}}$ below the band bottom determines the energy of bound state in spectrum (19).

($\omega - E_{\mathbf{K}}$) which determine spectrum (12) for the coverage $\Theta=0.7\%$, effective electron mass $m_e=1$, $d_{\text{nn}}=2.54 \text{ \AA}$ (4.80 a.u.), and two values of $|\mathbf{K}|=K$ that correspond to initial state electron energies of 0 and 13.6 meV above the IS band bottom denoted as $\omega=0$. The plots of $\Gamma_{\mathbf{K}}(\omega)$ and $\Lambda_{\mathbf{K}}(\omega)$ for wave vectors K corresponding to initial electron energies of 100 and 400 meV relevant to the experiments described in Ref. 17 exhibit qualitatively similar behavior. The most prominent characteristic of $\Gamma_{\mathbf{K}}(\omega)$ in both figures is a sharp drop from a finite value to zero at the band bottom. For large positive values of ω lying outside the plot range the values of $\Gamma_{\mathbf{K}}(\omega)$ fall off rapidly and this provides an effective cutoff equivalent to a finite bandwidth in all the integrals involving spectral density (12). This behavior is a direct consequence of the finiteness of scattering matrix element $V_{\text{IS}}(\mathbf{Q})$ for zero momentum transfer $\mathbf{Q}=0$ and the two-dimensional character of IS band. As a consequence, the real part of the self-energy $\Lambda_{\mathbf{K}}(\omega)$, given by the Hilbert transform of $\Gamma_{\mathbf{K}}(\omega)$ through Eq.

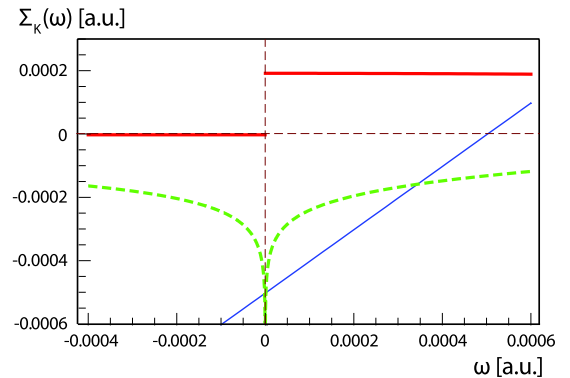


FIG. 4. (Color online) Same as in Fig. 3 but for initial wave vector $K=0.0316$ a.u. corresponding to electron energy $E_{\mathbf{K}} = 13.6$ meV. Note that for this value of initial electron energy there appears three intersections of $\Lambda_{\mathbf{K}}(\omega)$ with the line $\omega - E_{\mathbf{K}}$. The energy of leftmost intersection slightly below the band bottom determines the energy of bound state whereas the ones above the bottom give rise to complex poles (resonances) that give rise to maxima in the band part of spectrum (19).

(15), exhibits a two-sided logarithmic divergence at the band bottom and falls off asymptotically as $1/\omega$ for bands of finite effective width. All these characteristics of $\Gamma_{\mathbf{K}}(\omega)$ and $\Lambda_{\mathbf{K}}(\omega)$ profoundly affect the general features of quasiparticle spectrum (12).

In the subthreshold region $\omega < 0$ where $\Gamma_{\mathbf{K}}(\omega) = 0$ there will always exist an intersection of the logarithmically divergent $\Lambda_{\mathbf{K}}(\omega)$ with the line $\omega - E_{\mathbf{K}}$ (cf. Figs. 3 and 4). This gives rise to an isolated pole in spectrum (12) of the form

$$S_{\mathbf{K}}^B(\omega) = Z_{\mathbf{K}}^B \delta(\omega - \omega_{\mathbf{K}}^B) \quad (18)$$

at the value $\omega_{\mathbf{K}}^B$ satisfying the equation $[\omega_{\mathbf{K}}^B - E_{\mathbf{K}} - \Lambda_{\mathbf{K}}(\omega_{\mathbf{K}}^B)] = 0$, with the weight given by $Z_{\mathbf{K}}^B = 1/[1 - \partial\Lambda_{\mathbf{K}}(\omega_{\mathbf{K}}^B)/\partial\omega_{\mathbf{K}}^B]$. Hence the full spectrum (12) of an electron scattered by attractive impurities splits in two components, the simple pole contribution (18) below the IS-band bottom and the continuous part $S_{\mathbf{K}}^C(\omega)$ within the range of IS band. Hence, expression (12) takes the form

$$S_{\mathbf{K}}(\omega) = Z_{\mathbf{K}}^B \delta(\omega - \omega_{\mathbf{K}}^B) \theta(-\omega) + S_{\mathbf{K}}^C(\omega) \theta(\omega). \quad (19)$$

The appearance of subthreshold pole (18) in spectrum (19) signifies the existence of a bound electronic state (hence index B) localized by the scattering potential. Such bound states are generic of the 2D systems with attractive scattering potentials⁵¹ irrespective of the strength of interaction which can only affect the position $\omega_{\mathbf{K}}^B$ and spectral weight $Z_{\mathbf{K}}^B$ of the bound state. Their occurrence has been predicted for the interactions of quasi-two-dimensional electrons with surface defects in the various theoretical models^{27,29-31} and also confirmed experimentally in a number of systems.⁵²

The magnitude of $Z_{\mathbf{K}}^B$ in Eq. (19) diminishes rapidly as $E_{\mathbf{K}}$ is increased so that in going from $E_{\mathbf{K}} = 0$ meV to $E_{\mathbf{K}} = 13.6$ meV it drops from 0.666 to 0.0365. For low values of $E_{\mathbf{K}}$ for which there are no real intersections of the line $\omega - E_{\mathbf{K}}$ with $\Lambda_{\mathbf{K}}(\omega)$ in the band region $\omega > 0$, the pole of $S_{\mathbf{K}}^C(\omega)$ will lie far away from the real axis in the complex plane and the spectrum will exhibit a type of the behavior shown in Fig. 5. On the other hand, the intersections of $\Lambda_{\mathbf{K}}(\omega)$ with the line $\omega - E_{\mathbf{K}}$ for which $E_{\mathbf{K}} \gg \Lambda_{\mathbf{K}}(E_{\mathbf{K}})$ give rise to resonances whose widths are controlled by the values of $\Gamma_{\mathbf{K}}(\omega)$ at the intersection points. Such a situation is illustrated in Fig. 4. The intersection slightly above the band bottom gives rise to a narrow threshold resonance in the spectrum (cf. Fig. 6) whose weight rapidly decreases with the increase in $E_{\mathbf{K}}$, in the same fashion as does the weight $Z_{\mathbf{K}}^B$ of the bound state. In this case the majority of the spectral weight is associated with the pole appearing at the complex zero of the denominator of Eq. (12), whose real part is controlled by the intersection of $\omega - E_{\mathbf{K}}$ with the postlogarithmic part of $\Lambda_{\mathbf{K}}(\omega)$. This pole gives rise to a Lorentzian-type peak in the spectrum $S_{\mathbf{K}}^C(\omega)$ (cf. Figs. 6 and 7) and in the following will be referred to as the self-consistent FGR pole because its determination requires self-consistent solution of equations involving off-the-energy-shell values of $\Lambda_{\mathbf{K}}(\omega)$ and $\Gamma_{\mathbf{K}}(\omega)$. As will be shown below, the existence and characteristics of this pole determine temporal evolution of the excited quasiparti-

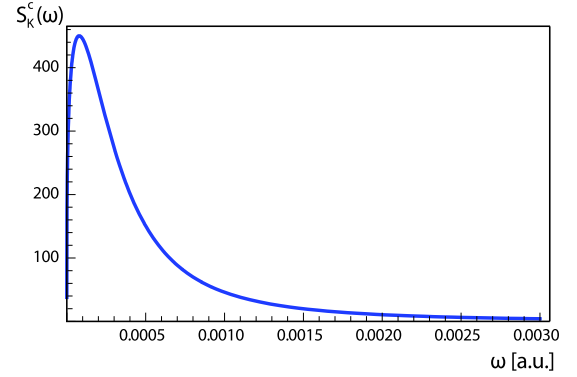


FIG. 5. (Color online) Band or continuous part of spectrum (19) for initial electron momentum $K=0$ or $E_{\mathbf{K}}=0$. The contribution of this part to the total spectral weight is 23.4% and the remainder is located in the bound state located at $\omega_{\mathbf{K}}^B = -0.000216$ a.u. $= -5.87$ meV below the band bottom. The FGR pole is not well defined for $E_{\mathbf{K}}=0$ and the spectrum is dominated by bound state (18) and threshold behavior (20).

cle over broad time scales. Another important general feature of Eq. (19) that arises from the 2D character of the scattering event is the threshold behavior

$$\lim_{\omega \rightarrow 0} S_{\mathbf{K}}^C(\omega) \propto \Theta(\omega)/(\ln \omega)^2 \quad (20)$$

which in turn determines the long time (asymptotic) behavior of the propagation amplitude through Eq. (11). The evolution of the discussed features of $S_{\mathbf{K}}^C(\omega)$ with the increase in $E_{\mathbf{K}}$ are illustrated in Figs. 5–7. For initial IS-electron energies $E_{\mathbf{K}} > 100$ meV the spectra are qualitatively similar to the spectrum shown in Fig. 7.

At this point it is important to notice that the above obtained characteristics of $\Gamma_{\mathbf{K}}(\omega)$ and $\Lambda_{\mathbf{K}}(\omega)$ also persist if higher-order terms in the self-energy proportional to higher

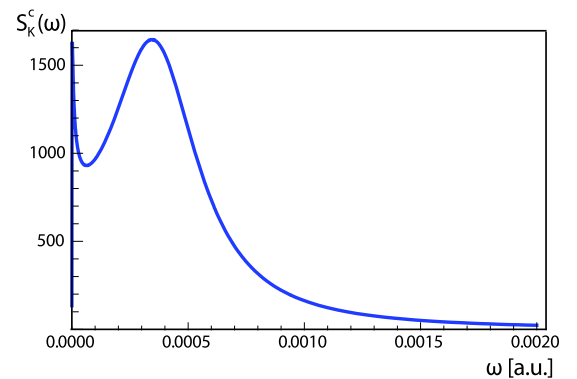


FIG. 6. (Color online) Illustration of the two-pole structure of the band part of spectrum (19) for initial electron momentum $K = 0.0316$ a.u. corresponding to the energy $E_{\mathbf{K}} = 13.6$ meV. The contribution of this part to the total spectral weight is 96.3% and the remainder is associated with the pole located at the bound-state energy $\omega_{\mathbf{K}}^B = -1.468 \times 10^{-6}$ a.u. $= -0.0399$ meV below the band bottom. The threshold resonance slightly above the band bottom has a small weight ($\approx 2.3\%$) relative to the FGR-pole-derived peak at $\omega \sim 0.0003$ a.u. (~ 8 meV).

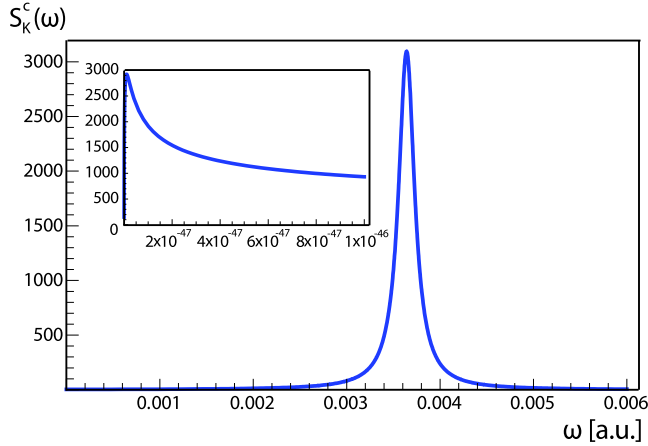


FIG. 7. (Color online) Same as in Fig. 6 but for initial electron momentum $K=0.0857$ a.u. corresponding to the energy $E_K=100$ meV. The spectrum is dominated by the FGR-pole-derived Lorentzian-shaped maximum whose position is to a good approximation determined by the zero of expression $[\omega - E_K - \Lambda_K(\omega)]$ in the postlogarithmic region. The bound state slightly below and the threshold resonance slightly above the band bottom (see inset) carry negligible spectral weight.

powers of the coupling constant (here the strength of electron-atom dipolar interaction) are taken into account. For small dipole strengths their effect amounts to producing corrections to the leading contributions given by Eqs. (14) and (15) and thereby to the values of bound state and band resonance energies and intensities, etc., but not to changes in the general characteristics of spectrum (12) and the corresponding electron propagation amplitude (11). Therefore, the general behavior of quasiparticle survival probability may be assessed using Eqs. (11)–(20) with a proviso that in the presence of IS-electron interactions with electrons in other bands of a real three-dimensional (3D) system both the subthreshold bound state would be resonantly broadened and the band states additionally broadened by interband transitions and dynamical interactions.^{29,38,39}

The effects of resonant broadening of bound state (18) on propagation amplitude (1) cannot be assessed from the present one-band approach. They can be modeled²⁹ by adding a phenomenological exponentially decaying factor to $G_K^B(t)$ obtained by applying Eq. (11) to Eq. (18), viz.

$$G_K^B(t) \rightarrow Z_K^B \exp(-i\omega_K^B t - \Delta^B t/2) \Theta(t). \quad (21)$$

Such a modified $G_K^B(t)$ complements the contribution $G_K^c(t)$ arising from the band part of spectrum $S_K^c(\omega)$ in Eq. (19). Here Δ^B is the value of bound-state resonance full width at half maximum (FWHM) that should be estimated or calculated separately from multiband models or taken from experiment. Note that this ansatz is equivalent to treating the interband transitions at the FGR level which, in view of the large widths of bulk bands, may represent a reliable approximation. In the following discussion we shall adopt the value $\Delta^B=14$ meV used in Ref. 29. With these prerequisites one can discuss general features of the evolution of excited quasiparticles using Eqs. (2)–(6) and (11). Quite generally, the

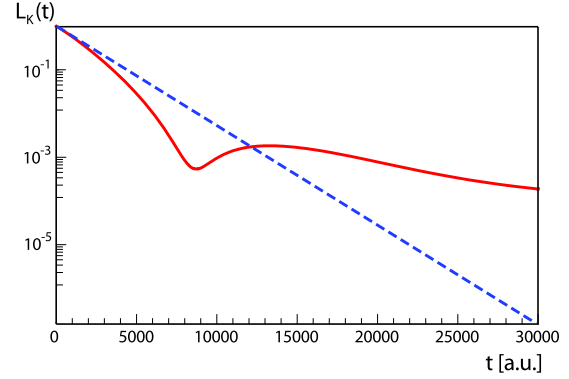


FIG. 8. (Color online) IS-electron survival probability $L_K(t)$ as a function of time (1 a.u.= 2.4189×10^{-2} fs or 1 fs= 41.34 a.u.) for initial quasiparticle momentum $K=0$. The dashed curve is the bare FGR decay described by expression (22). Note logarithmic scale on the vertical axis. Notable in the depicted behavior of $L_K(t)$ is the absence of an intermediate evolution interval during which the survival probability could be well approximated by the FGR decay. Here the early Zeno behavior (23) is directly superseded by the nonexponential dephasing (28) at around $t=8000$ a.u. (~ 200 fs).

excited quasiparticle evolves through three distinct intervals characterized by different types of temporal behavior. The physics underlying these distinct types of evolutions is discussed below.

Evolution of the IS-electron survival probabilities for three different initial momenta corresponding to the band energies of 0, 100, and 400 meV are shown in Figs. 8–10, respectively. Also shown for comparison are the FGR-derived survival probabilities

$$L_K^{\text{FGR}}(t) = \exp[-2\Gamma_K(E_K)t] = \exp(-t/\tau_K^{\text{FGR}}), \quad (22)$$

with the on-the-energy-shell values of $2\Gamma_K(E_K)$ calculated for the same initial quasiparticle momenta (cf. Fig. 2). The

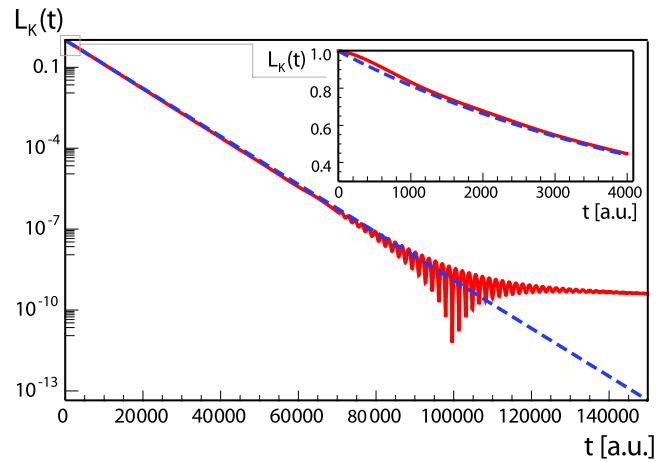


FIG. 9. (Color online) Same as in Fig. 8 but for initial quasiparticle momentum $K=0.0857$ a.u. corresponding to the energy $E_K=100$ meV. Here a strong interference between exponential and postexponential dephasings that cause survival collapse extend over the interval $\sim 70\,000$ – $130\,000$ a.u. (~ 1750 – 3250 fs). The inset shows the early Zeno behavior (23).

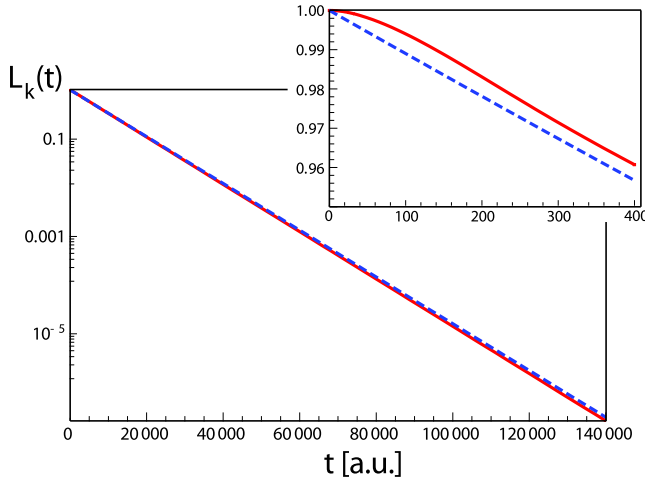


FIG. 10. (Color online) Same as in Fig. 9 but for initial quasiparticle momentum $K=0.172$ a.u. corresponding to the energy $E_{\mathbf{K}}=400$ meV. The survival collapse is not reached on the time scale of the plot ~ 3400 fs. Inset: Blow up of the early Zeno decay (23) shown on the time scale of 400 a.u. (~ 10 fs).

early evolution of the quasiparticle state is governed by the Heisenberg energy uncertainty which gives rise to a quadratic initial decay of the survival probability known as the “quantum Zeno effect”^{49,53}

$$L_{\mathbf{K}}(t) \sim 1 - t^2/\tau_Z^2 + \mathcal{O}(t^4). \quad (23)$$

Here the so-called Zeno time is given by

$$\tau_Z^{-2} = (\mu_2 - \mu_1^2), \quad (24)$$

where μ_1 and μ_2 are the first and second energy moments of spectrum (12), respectively. For the studied system both moments are finite and produce the Zeno time in accord with time-dependent perturbation theory^{54,55}

$$\tau_Z^{-2} = \frac{1}{\pi} \int_0^\infty d\omega \Gamma_{\mathbf{K}}(\omega) = \langle \mathbf{K}, \text{IS} | V^2 | \mathbf{K}, \text{IS} \rangle_c, \quad (25)$$

where V^2 comprising interaction (9) is ensemble averaged over the impurities in the same fashion as the second-order self-energy diagram in Fig. 1. This yields the contribution linearly proportional to defect concentration c [hence subscript c associated with the matrix element on the right-hand side (RHS) of expression (25)] from which the processes of consecutive forward scattering by different adatoms that lead to c^2 contributions are excluded. Therefore,

$$\tau_Z \propto c^{-1/2}. \quad (26)$$

In the present one-band model in which the $|\mathbf{K}\rangle$ states are 2D plane waves the matrix element on the RHS of expression (25) turns out independent of the initial electron wave vector \mathbf{K} (and thereby of the initial energy within the IS band), as one would expect for ballistic motion, and for the adatom coverage $\Theta=0.7\%$ yields $\tau_Z=22.9$ fs.

As is clear from the expression for the Zeno time, the early decay is affected only by the gross features (i.e., moments) of the spectrum because the energy conservation cannot be established during the ultrashort initial evolution pe-

riod of the order of the inverse band width. In calculating these moments in the present one-band model one should also take care to represent the bound-state spectrum by Eq. (18) and use expression (21) only in the sum with the Fourier transform of the continuous part of spectrum (12) in order to suppress unphysical saturation of the survival probability for $t \rightarrow \infty$ at the value $(Z_{\mathbf{K}}^B)^2$.

As the duration of evolution grows longer the energy conservation sets in and the scattering processes become more and more constrained to the energy shell. This is the period in which the quasiparticle survival probability becomes dominantly affected by the poles of spectrum (12) in the lower part of the complex ω plane that determine the *self-consistent* scattering rates (14) and energy shifts (15), as well as the appearance of bound state (18) arising from the multiple scattering processes. In the present one-band model description of a two-dimensional electron system there arise three poles from zeros of the denominator of expression (12): a pole at the energy of the already discussed bound state for negative $\omega=\omega_{\mathbf{K}}^B$, its counterpart across the band bottom which appears as a result of intersection of $\omega-E_{\mathbf{K}}$ with the logarithmically divergent threshold part of $\Lambda_{\mathbf{K}}(\omega)$, and the FGR pole from the intersection of $\omega-E_{\mathbf{K}}$ with the post-threshold part of $\Lambda_{\mathbf{K}}(\omega)$. Since the weight of the FGR pole increases rapidly with the increase in $E_{\mathbf{K}}$ the decay of quasiparticle survival probability will in this case be dominantly exponential, in accord with a standard picture of quasiparticle propagation in the band.

The spectral structure around the FGR pole determines the regime of steady state decay of the quasiparticle typical of Markovian dynamics which for large values of K behaves as

$$L_{\mathbf{K}}^{\text{sc}}(t) = a_{\mathbf{K}} \exp(-2\Gamma_{\mathbf{K}}^{\text{sc}}t) = a_{\mathbf{K}} \exp(-t/\tau_{\mathbf{K}}^{\text{sc}}). \quad (27)$$

Here $a_{\mathbf{K}}$ is the quasiparticle weight in the region of exponential decay given by the absolute square of the residue of FGR pole determined as the rightmost self-consistent zero $\Lambda_{\mathbf{K}}^{\text{sc}} - i\Gamma_{\mathbf{K}}^{\text{sc}}$ of the denominator of Eq. (12). Here the deviation of the survival probability from the simple exponential law (22) is small and hence the concept of a scattering cross section calculated from the *bare* FGR transition rate (17) is applicable. It is also noteworthy that the crossover from Zeno to self-consistent FGR type of behavior [Eq. (27)] is smooth in all the cases considered. A systematic decrease in both $\Gamma_{\mathbf{K}}^{\text{sc}}$ and on-the-energy-shell $\Gamma_{\mathbf{K}}(E_{\mathbf{K}})$ with the increase in K is in accord with the earlier reported¹⁷ behavior of $\sigma_{\mathbf{K}}$ defined by Eq. (17). However, it should be noted that for very small initial K 's the contribution from the FGR pole may be missing or insufficient to produce a long-lasting exponential dephasing and the initial Zeno decay is in that case directly taken over by the asymptotic decay. As is evident in Fig. 8, for $K=0$ this takes place already around 8000 a.u. (≈ 200 fs). In this context it should also be noted that the characteristic lifetimes introduced in Eqs. (23) and (27) which govern the quasiparticle decay in the Zeno and FGR regimes exhibit different scaling with the concentration c of scatterers, viz. $\tau_Z \propto 1/\sqrt{c}$ and $\tau_{\mathbf{K}}^{\text{sc}} \propto 1/c$. Hence, the crossovers from one regime to the other are generally affected by the

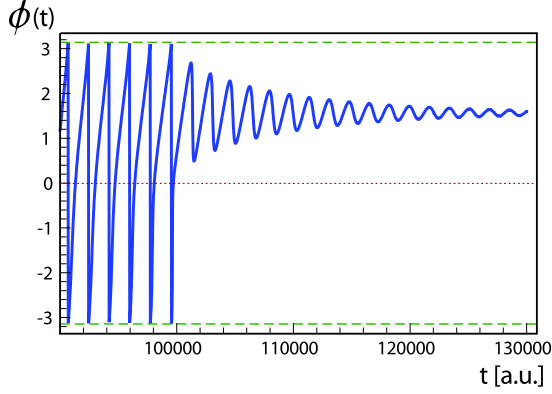


FIG. 11. (Color online) Evolution of the phase $\phi(t)$ (modulo 2π) of the survival amplitude [see Eqs. (6) and (3)] of IS electron for initial momentum $K=0.0857$ a.u. corresponding to the energy $E_{\mathbf{K}}=100$ meV shown in the range $90\,000 < t < 130\,000$ a.u. ($\sim 2200 < t < 3000$ fs). In this interval the corresponding survival probability shown in Fig. 9 exhibits a survival collapse and cross-over from the FGR to the asymptotic decay. The initial quasiparticle phase grows linearly with time as $-i\phi(t) = -iE_{\mathbf{K}}t$ but in the cross-over interval starts oscillating around a finite asymptotic value. In this interval the initial quasiparticle identity is lost.

variation of c and this property may be used to easier access and discern these intervals experimentally.

For yet longer evolution intervals the propagating quasiparticle explores the details of the spectral structure near the band bottom because for long times the destructive interference between the states in that region is smaller than for the states farther away from the threshold. Here the peculiar threshold behavior of spectrum (20) gives rise to a contribution to the survival probability that asymptotically goes as

$$\lim_{t \rightarrow \infty} L_{\mathbf{K}}(t) \propto \frac{1}{t^2 (\ln t)^4}, \quad (28)$$

i.e., falls off slower than the contribution from the poles that decay exponentially. Whereas the asymptotic inverse power-law decay of the survival probability was predicted long ago^{56–59} and derived for a variety of model systems,^{49,54} the appearance of additional logarithmic factor⁶⁰ in Eq. (28) is generic of 2D systems. Here it should be noted that the cross-over from self-consistent FGR type of dephasing [Eq. (27)] to asymptotic behavior [Eq. (28)] is not smooth but rather characterized by a collapse of the survival probability^{49,54} due to strong interferences between the contributions from two distinct evolution intervals. This is clearly visible in Fig. 9 where the survival probability first reaches a minimum around $100\,000$ a.u. ≈ 2500 fs and then recovers through oscillations before reaching the asymptotic decay (28). Such behavior reflects a drastic change in the phase of survival amplitude (3) which beyond the crossover interval loses the simple quasiparticle features determined by the FGR pole of spectrum (12). This is illustrated in Fig. 11.

As is illustrated in Figs. 8–10, a striking qualitative and quantitative difference arises between the survival probabilities and bare exponential FGR-derived decay of initial electron states with lower excitation energies (i.e., small initial

wave vectors). There are two main sources of such a behavior. One is the presence of the bound state whose contribution may alter the survival probability (22) calculated by taking into account only the band states as final scattering states. The other is the effect of band bottom which induces different quantum interferences between the electron states near the excitation threshold than higher up in the band where the one-pole approximation for the spectral density based on the dominance of FGR pole (cf. Fig. 7) yields the self-consistent FGR dephasing rate.⁴⁹ These points will be further discussed in Sec. V.

III. CALCULATION OF THE QUASIPARTICLE SURVIVAL PROBABILITY IN THE WAVE-PACKET PROPAGATION APPROACH

In this section we address the problem of dynamics of electrons excited into IS band by considering a 2D one-particle Schrödinger equation in the coordinate representation

$$i \frac{\partial \Psi(x, y, t)}{\partial t} = - \frac{\nabla^2}{2m_e} \Psi(x, y, t) + V(x, y) \Psi(x, y, t), \quad (29)$$

in which the 2D potential $V(x, y)$ describes electron interactions with impurities (adsorbates) randomly distributed over the surface plane. In accordance with Sec. II, all quantities are expressed in atomic units and the effective mass of IS electron is $m_e=1$. The total potential $V(x, y)$ is obtained as

$$V(x, y) = \sum_j \langle \psi_{IS}(z) | V(\mathbf{R} - \mathbf{R}_j) | \psi_{IS}(z) \rangle = \sum_j V_j(\mathbf{R}), \quad (30)$$

where the potential of a single scattering center $V_j(\mathbf{R})$ is the same as used in the self-energy approach of Sec. II. The positions of the scattering centers \mathbf{R}_j are chosen at random (with respect to the uniform probability distribution), and an example of a single realization of this distribution is depicted in Fig. 12.

The dynamics of IS electron is described by the time-dependent wave function $\Psi(x, y, t)$. To study the evolution of electrons which are initially excited into momentum eigenstates in IS bands, we start from the initial-state wave function $\Psi_{\mathbf{K}}(x, y, t=0) = \exp(i\mathbf{K}\mathbf{R}) / \sqrt{L^2}$. Since this is not an eigenstate of the system with impurities, subsequent electron dynamics depends on the potential $V(x, y)$. From this the survival probability of the initial electron state is obtained in the form

$$L_{\mathbf{K}}(t) = \left| \int dx dy \Psi_{\mathbf{K}}^*(x, y, 0) \Psi(x, y, t) \right|^2, \quad (31)$$

which is simply Eq. (2) with the wave functions represented in coordinate representation. The evolution of the thus defined $L_{\mathbf{K}}(t)$ depends on the specificities of the potential V_j of

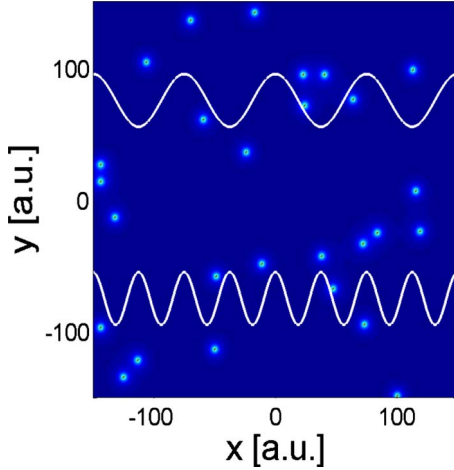


FIG. 12. (Color online) Single realization of a potential $V(x,y)$ describing randomly distributed scattering centers depicted in an area of 300×300 Bohr radius squared. The concentration is $c = 0.0003$ a.u. The white solid lines depict the functions $\text{Re exp}(iKx)$, where $K=0.0836$ and $K=0.1672$ a.u. (see text).

a single scattering center, concentration of the scatterers c , and the magnitude of initial momentum $K=|\mathbf{K}|$. In our numerical simulations of electron scattering by random arrays of impurities we assume periodic boundary conditions in a square box of area L^2 so that the number of scattering centers in the box is $N=cL^2$ (cf. Sec. II). The electron dynamics is assessed by solving Eq. (29) numerically with the use of standard split-step Fourier technique to evaluate $\Psi(x,y,t) = \exp(-iHt)\Psi_{\mathbf{K}}(x,y,0)$ from the initial-state wave function. Due to the finite size of the present system, evolution of $L_{\mathbf{K}}(t)$ depends also on a particular distribution of the scattering centers. In order to gain insight into the dynamics beyond this effect numerical simulations must be repeated several times, each time with a different realization of the defect distribution. It is reasonable to assume that for an infinite generic system the converged temporal evolution would correspond to the values obtained by averaging over many possible realizations of the scattering centers. As an illustration of the relation between concentration and wavelength of the initially excited electron, Fig. 12 also displays $\text{Re exp}(iKx)$ for $K=0.0836$, and $K=0.1672$ a.u.

In the following we present the results of a series of simulations that explore the behavior of $L_{\mathbf{K}}(t)$ for three values of the initial-state wave vector, $K=0$, $K=0.0836$, and $K=0.1672$ a.u., which correspond to the energies of 0, 95, and 380 meV, respectively. Figures 13–15 show the survival probability obtained for concentration $c=0.0003$ a.u. (corresponding to experimental $\Theta=0.7\%$ in Ref. 17) which is identical to that of Sec. II and calculated on a numerical grid of 256×256 points on an area corresponding to 300×300 a.u. Figure 13 shows $L_{\mathbf{K}}(t)$ for $K=0$ for three different realizations of the scattering centers and $c=0.0003$. Similarly, Figs. 14 and 15 show $L_{\mathbf{K}}(t)$ for $K=0.0836$ a.u. and 0.1672 a.u., respectively. These figures demonstrate that there is a fairly large numerical window in which the decay of the initial state $\Psi_{\mathbf{K}}(x,y,0)$ is governed by Fermi's golden rule. Numerical fits of these curves within the FGR window

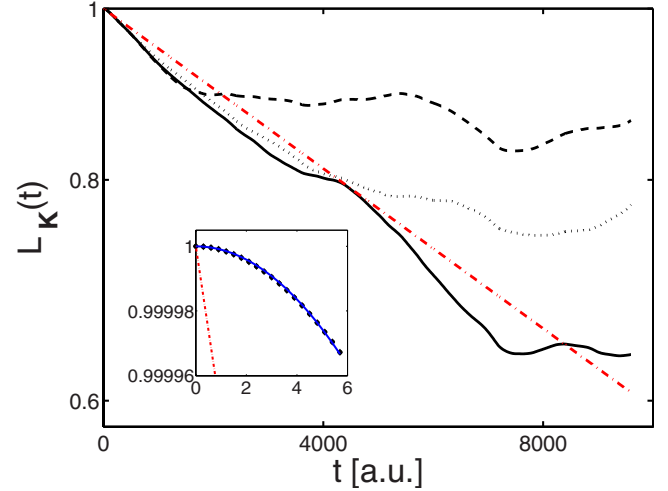


FIG. 13. (Color online) Survival probability $L_{\mathbf{K}}(t)$ for $K=0$ at low density of the scattering centers, $c=0.0003$ a.u. The three curves correspond to three different configurations of the scattering centers. The dot-dashed line is the fitted FGR decay $\exp(-2\Gamma t)$ with $2\Gamma=0.52 \times 10^{-4}$ a.u. (see text and Fig. 2). The inset shows the computed early decay (symbols) and fits (full line) to quadratic Zeno behavior (23) which yields $\tau_Z=988$ a.u.=23.9 fs. The dot-dashed line is the same as in the main plot.

show that decay rates for the three calculated momenta are approximately 0.52×10^{-4} , 1.31×10^{-4} , and 0.86×10^{-4} a.u. for $K=0$, $K=0.0836$, and $K=0.1672$ a.u., respectively. Despite the fact that these values were obtained from a limited number of simulations and therefore are expected to exhibit a large scatter, they are of the same order as the ones obtained within the FGR approach in Sec. II (see Fig. 2).

In the self-energy approach of Sec. II we have only treated the scattering processes linear in the concentration c of impurities by systematically neglecting contributions from the self-energy terms proportional to higher powers of c , which is justified for low concentrations. On the other hand,

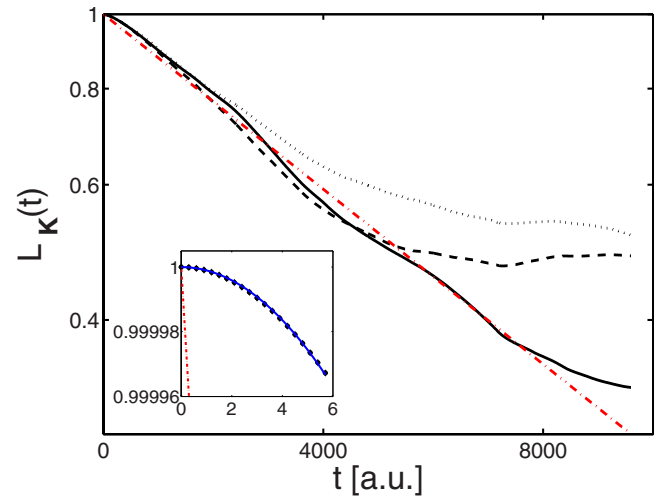


FIG. 14. (Color online) Same as in Fig. 13 but for $K=0.0836$ a.u. The dot-dashed line is the fitted FGR decay $\exp(-2\Gamma t)$ with $2\Gamma=1.31 \times 10^{-4}$ a.u. (see text and Fig. 2).

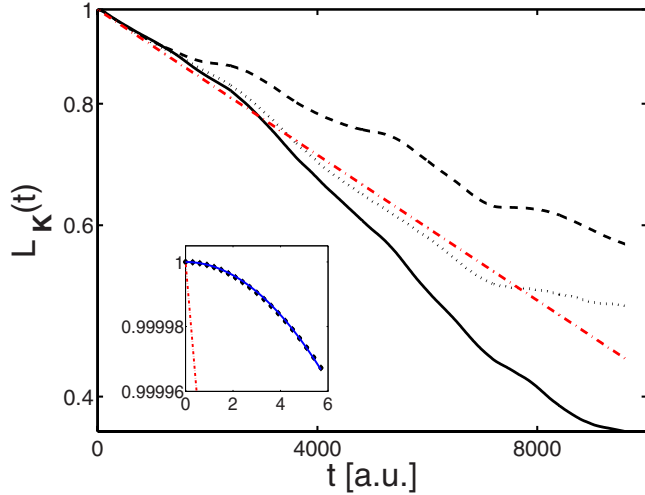


FIG. 15. (Color online) Same as in Fig. 14 but for $K=0.1672$. The dot-dashed line is the fitted FGR decay $\exp(-2\Gamma t)$ with $2\Gamma = 0.86 \times 10^{-4}$ a.u. (see text and Fig. 2).

by repeating the same simulations with much higher concentration, $c=0.007$ a.u., we find that the FGR decay is not nearly as dominant decay mode as at small concentrations. In this case the FGR decay is superseded by a much *earlier* collapse of the survival probability which again manifests itself as a sharp decrease in $L_{\mathbf{K}}(t)$ in a narrow time interval.

The present simulations also enable us to explore the early Zeno decay (see insets of Figs. 13–15) and the variation of Zeno time with the concentration of scatterers beyond the framework of the model discussed in Sec. II. Figure 16 shows τ_Z as a function of concentration in the experimental range of Ref. 17. These results support the findings of Sec. II both qualitatively ($\tau_Z \propto 1/\sqrt{c}$ and independent of initial \mathbf{K}) and quantitatively within the numerical accuracy.

Additional insight into the dynamics of scattering processes with different initial wave vector can be obtained by inspecting the evolution of Fourier momentum spectrum

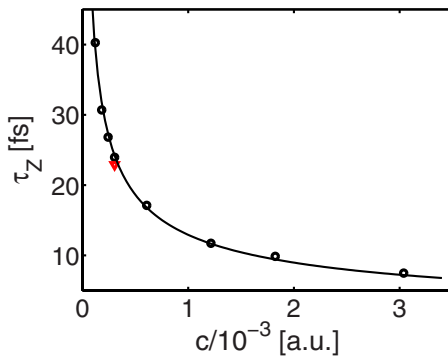


FIG. 16. (Color online) Numerical values of the Zeno time as a function of concentration of scatterers. Data are extracted from simulations of the quasiparticle survival probability (31) using expression (23). The full curve is a power-law fit to numerical values which yields $\tau_Z = 0.339c^{-0.527}$ fs, in very good agreement with the analytical result $\tau_Z \propto c^{-1/2}$ derived in Sec. II. The inverted triangle is the value of τ_Z obtained in Sec. II for the concentration $c=0.0003$ ($\Theta=0.7\%$).

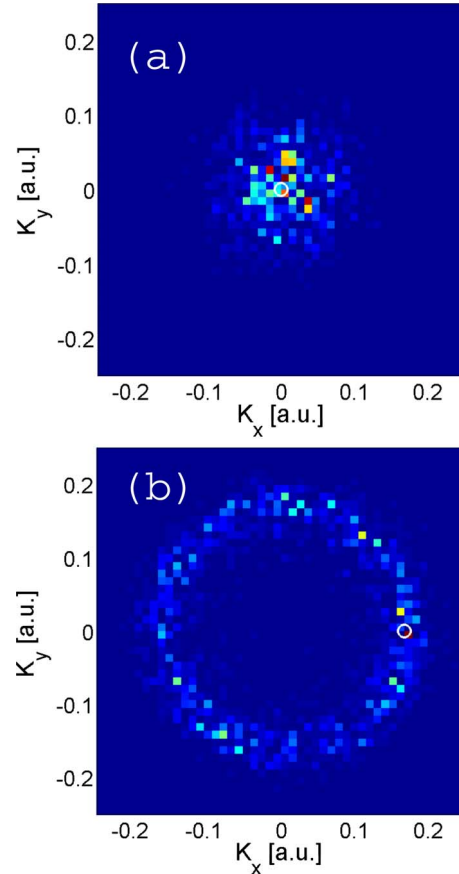


FIG. 17. (Color online) (a) The momentum spectrum of the wave function at time $t=0$ (small open circle), and at time $t=80$ fs. The initial wave function corresponds to the wave vector magnitude $K=0$. (b) Same as in (a) but for the wave function with initial wave vector magnitude $K=0.1672$ a.u. (small open circle) pointing in the x direction. The radius of the big K' circle is equal to initial K (see text for details).

of the wave functions $P(\mathbf{K}, t) = |\tilde{\Psi}(K_x, K_y, t)|^2$, where $\tilde{\Psi}(K_x, K_y, t)$ is the Fourier transform of the wave function $\Psi(x, y, t)$ with respect to spatial coordinates. Figure 17 shows quasiparticle momentum relaxation, viz. the evolution of momentum spectra with initial $K=0$ and $K=0.1672$ a.u. for a single-shot propagation for the concentration of scatterers $c=0.007$ a.u. Here we clearly see the spread of the projection of perturbed wave function in the course of time over the band eigenstates $|\mathbf{K}'\rangle$ of the unperturbed Hamiltonian. The projections with the largest weight are peaked around the unperturbed wave functions with the magnitude of the wave vectors equal to that of the initial state, viz. $|\mathbf{K}'|=K$.

Finally, let us briefly comment on some important aspects of the present simulations. In contrast to the self-energy method employed in Sec. II, the numerical wave-packet propagation method can treat larger concentrations easier and with higher accuracy, mainly because the decrease in the survival probability occurs on shorter time scales. Thus, one can use larger numerical grids covering greater area with the same accuracy. For larger areas and larger defect concentrations the finite-size effects become less important. Also, for larger concentrations a smaller numerical area L^2 is in-

fluenced by the finite-size effects. In this sense, the self-energy method and the present numerical method of wave-packet propagation are complementary.

IV. CALCULATION OF THE QUASIPARTICLE SURVIVAL PROBABILITY IN THE TIGHT-BINDING APPROACH

In this section we extend our studies of IS-electron dynamics by mapping the impurity scattering problem described by a 2D Schrödinger equation (for clarity we restore the factor \hbar)

$$-\frac{\hbar^2}{2m_e}\nabla^2\Psi(x,y) + V(x,y)\Psi(x,y) = E\Psi(x,y) \quad (32)$$

onto a tight-binding representation of electron dynamics. This is achieved by discretizing spatial coordinates x and y in Eq. (32) which enables establishing a tight-binding model of the system similar to the ones employed in earlier studies of non-Markovian electron dynamics.⁴⁹ By choosing a square mesh with the size of 2D square lattice a in both directions we obtain the discretized representation of Eq. (32) in the form

$$-\frac{\hbar^2}{2m_e a^2}[\Psi(x+a,y) + \Psi(x-a,y) + \Psi(x,y+a) + \Psi(x,y-a)] + \left[V(x,y) + 4\frac{\hbar^2}{2m_e a^2} - E \right] \Psi(x,y) = 0. \quad (33)$$

This equation can be interpreted as a diagonalization condition for the tight-binding Hamiltonian defined as

$$H = \sum_i E_i |i\rangle\langle i| + \sum_{i,j} \varepsilon |i\rangle\langle j|, \quad (34)$$

where $E_i = V_i + 4\hbar^2/(2m_e a^2)$, $\varepsilon = -\hbar^2/(2m_e a^2)$, and indices i and j count the sites in a square lattice. The hopping is allowed only to the nearest-neighbor lattice sites. This means that the number of lattice sites corresponds to the number of Cu atoms in the Cu(001) surface plane. Note that the potential appears in the diagonal part as a component of the site “orbital” energy, whereas the kinetic energy appears in the off-diagonal part (hopping term) of the Hamiltonian.

Any potential can be represented on a square mesh by additive renormalization of the orbital energy by $V_i = V(x_i, y_i)$ where (x_i, y_i) are the coordinates of the i th site. To represent the dipole potential fixed to a certain site, one should in principle renormalize all the sites in a mesh due to the infinite range of the potential. We shall, however, represent the effect of the dipole potential of an adatom only on a *single* adsorption site. The reason for this is that the thus obtained Hamiltonian can be most easily interpreted as the so-called diagonal disorder Hamiltonian studied previously in the context of Anderson’s localization (see, e.g., Refs. 61 and 62). In order to represent the adatom dipole potential by a single-site contact potential of the tight-binding model we shall renormalize the energy of an array of impurity sites by $\Delta V_i = 3V(Q=0)/(2a^2)$, where $V(Q=0)$ is the matrix element of the potential for zero lateral momentum transfer (i.e., integral of the potential over lateral coordinates). This expression has an obvious geometrical interpretation in terms of the integral of the potential, i.e., the volume of “dipole potential pyramid” erected above a particular lattice site. Note that the potential scales with a^{-2} as does the hopping matrix element ε . In all the following calculations we put $a = d_{\text{nn}} = 2.54 \text{ \AA}$ [i.e., the nearest-neighbor spacing in the Cu(001) plane]. By using such a model with the long-range dipolar potential replaced by the on-site contact potential we do not expect to

retrieve the energy dependence of decay rates as found in Secs. II and III. What we do expect from using this model, however, is the possibility of treating large assemblies of random impurities on surfaces in fast converged calculations influenced little by the boundaries of the system. This enables exploring long propagation times and thereby the effects of impurity concentration on the global behavior of quasiparticle survival probabilities.

Conceptually the simplest approach to dynamics governed by the Hamiltonian defined in Eq. (34) would be via its eigenvalues and eigenvectors. From this information one can easily construct temporal evolution of an arbitrary initial state.⁶² However, the need for diagonalization of the Hamiltonian matrix restricts the usefulness of this method to rather small sizes of the lattice (about $100 \times 100 = 10^4$ sites). To avoid the effects of finite size of the system on the temporal evolution, larger system sizes are required. To this end, adequate numerical approaches must be implemented. One possible approach consists of separating the Hamiltonian as

$$H = T + V, \quad (35)$$

where T and V are the kinetic and potential energy operators, respectively, and using this form for construction of the evolution operator of the system $\exp(-iHt/\hbar)$. The potential energy operator is represented by a diagonal matrix which can be exactly exponentiated. For the exponentiation of the off-diagonal kinetic energy operator we use the space-partitioning algorithm (see, e.g., Ref. 63). This permits exact exponentiation of T . Then, the dynamics is assessed by repeated operation of the exponentiated potential and kinetic energy matrices within a small time interval, Δt , so that the propagation of the wave function is obtained from

$$\begin{aligned} |\Psi(t + \Delta t)\rangle &= \exp\left(-i\frac{\Delta t}{\hbar}H\right)|\Psi(t)\rangle \\ &\approx \exp\left(-i\frac{\Delta t}{\hbar}T\right)\exp\left(-i\frac{\Delta t}{\hbar}V\right)|\Psi(t)\rangle. \end{aligned} \quad (36)$$

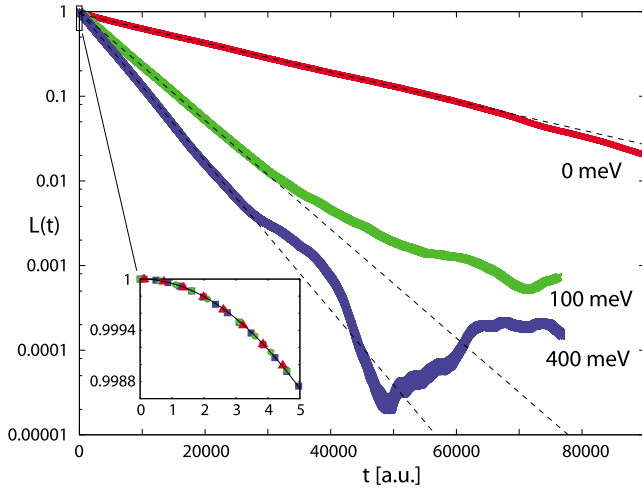


FIG. 18. (Color online) Survival probabilities of three eigenstates diagonalizing the adsorbate-free lattice Hamiltonian for initial energies E of 0, 100, and 400 meV (shaded lines). The number of lattice sites is 4 000 000, and the number of adsorbates is 28 000 ($\Theta=0.7\%$). The dashed lines are fits to form (22). The inset shows the early Zeno decays for initial $E_K=0$ meV (triangles), $E_K=100$ meV (circles), and $E_K=400$ meV (squares), which all follow the universal curve (23) independent of E_K .

In the limit $\Delta t \rightarrow 0$, Eq. (36) becomes exact (in matrix representation this is the so-called Trotter's product formula⁶³). In numerical calculations, the time step Δt must be carefully chosen such that the approximate equality in the second line of expression (36) holds to high degree of accuracy and that none of the important aspects of time dependence be influenced by this approximation. The method that we use can be easily and accurately applied to lattices containing tens of millions of sites (several thousands of sites along one side of a square lattice).

The wave function (36) can be written as an array of complex values $c_i(t)$, one per each site i of the lattice

$$|\Psi(t)\rangle = |c_1(t), c_2(t), \dots, c_N(t)\rangle, \quad (37)$$

where N is the total number of sites. In the limit when $N \rightarrow \infty$, the state vector becomes a two-dimensional complex function $\Psi(x, y, t)$. Hence, in the lattice representation the survival probability becomes

$$\begin{aligned} L(t) &= |\langle \Psi(0) | \Psi(t) \rangle|^2 \\ &= |\langle c_1(0), c_2(0), \dots, c_N(0) | c_1(t), c_2(t), \dots, c_N(t) \rangle|^2 \\ &= \left| \sum_{i=1}^N c_i(0)^* c_i(t) \right|^2, \end{aligned} \quad (38)$$

where $|\Psi(0)\rangle$ diagonalizes Hamiltonian (34) in the absence of renormalization potentials ΔV_i . Using this approach we consider the same examples of IS-electron evolution as in Secs. II and III for three initial electron energies of 0, 100, and 400 meV.

Figure 18 shows the survival probability of the eigenstates of lattice Hamiltonian (34) that are perturbed by random renormalizations ΔV_i at 0.7% of the sites in a square lattice

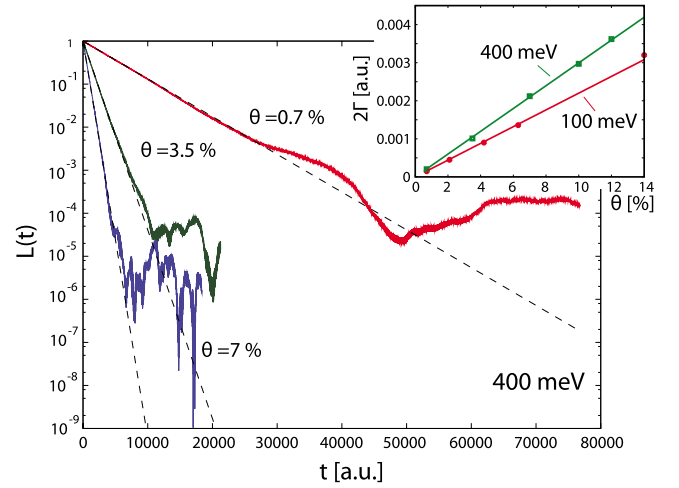


FIG. 19. (Color online) Survival probabilities of states diagonalizing the adsorbate-free lattice Hamiltonian for $E=400$ meV and three different adsorbate coverages ($\Theta=0.7\%$, $\Theta=3.5\%$, and $\Theta=7\%$) as denoted in the figure. The number of lattice sites is 4 000 000. The inset shows the decay rates in the exponential (FGR) regime (dashed lines in the body of the figure) as functions of the coverage of defects for initial energies of 100 and 400 meV.

comprising $2000 \times 2000 = 4\,000\,000$ sites. These results substantiate the global trends in the behavior of survival probability found in Secs. II and III, viz. the early quadratic decay independent of initial energy (see inset of Fig. 18) followed by the corrected exponential decay (27) in the intermediate region. Fits of the curves in the intermediate region to expression (27) yield $L_E = 0.94 \exp(-0.0000395t)$ for $E=0$ meV, $L_E = \exp(-0.000148t)$ for $E=100$ meV, and $L_E = \exp(-0.000203t)$ for $E=400$ meV, with t measured in a.u. of time. By further increasing E we have found that in the tight-binding model with random scattering centers represented by contact potentials the extracted $2\Gamma_E$ is an ascending function of the initial quasiparticle energy E , in contrast to the results of Secs. II and III. However, this should not be surprising in view of the use of a contact impurity potential which in the \mathbf{K} space corresponds to a constant and therefore according to Eq. (16) produces the decay rate proportional to the density of states that increases with energy in the lower half of the tight-binding band.

We recall that the formalism developed in Sec. II was employed under the assumption of low concentration of impurities which then yields the decay rates that are linearly proportional to concentration c of the scatterers. The applicability of this limit may be tested by numerical calculations outlined in this section. In Fig. 19 we show survival probabilities of a state with energy of 400 meV for three different adsorbate concentrations. The proportionality of the decay rate with adsorbate concentration holds up to an order of magnitude larger concentration than the ones studied experimentally.^{17,18}

V. DISCUSSION

Theoretical studies of electron-adsorbate scattering in surface bands carried out in the preceding sections by employ-

ing three complementary quantum-mechanical formalisms enable establishing a global picture of excited quasiparticle dynamics in the presence of low density of adatoms. The wave functions (or propagators) of electrons promoted into eigenstates within quasi-two-dimensional bands are strongly perturbed by the electron-adatom interactions even at small adatom concentrations. This results in the modification of amplitude and phase of the quasiparticle wave function both on the ultrashort (femtosecond) and asymptotic (picosecond) time scale. Thus, quite generally, upon promotion of a quasiparticle into a state sufficiently above the band bottom its subsequent evolution proceeds through three distinct intervals in which the quasiparticle dynamics is discernibly different. Using the quasiparticle survival probability (absolute square of propagators) and phase to characterize these intervals, we are able to identify the following regimes of quasiparticle motion in the presence of adsorbates: (i) Early quadratic or ballistic decay of the quasiparticle initial state (“quantum Zeno effect”) that is governed by the Heisenberg uncertainty principle. The rate of the ballistic decay or Zeno time (25) depends only on the gross features of the perturbed system (energy moments of the spectrum, band widths, etc.) in accord with the time-energy uncertainty principle. However, the duration of ballistic decay is not determined by the Zeno decay time but rather by the onset of on-the-energy-shell scattering processes. (ii) Intermediate or exponential decay determined by a modified, self-consistent Fermi golden rule decay rate describing on-the-energy-shell electron-adsorbate scattering processes [cf. Eq. (27)]. This intermediate evolution smoothly succeeds the Zeno decay and may extend over several thousands of femtoseconds, with a duration growing longer as the initial quasiparticle energy is increased. The corresponding decay rate and weight appear, respectively, as twice the imaginary part of the isolated pole and the square of its residue in the continuous part of the quasiparticle energy spectrum above the band bottom. The attractive dipolar electron-adsorbate interaction also generates localization of a fraction of excited electron in a bound state close below the band bottom but this effect rapidly diminishes with the increase in electron initial energy. (iii) For long propagation intervals the quasiparticles start to explore larger parts of the band with increasing phase and amplitude variations. This gives rise to interference between the various multiple scattering processes and leads to a collapse of the initial-state survival probability. After this the amplitude and phase of the quasiparticle propagator change so drastically that the initial quasiparticle identity is completely lost.

Our results demonstrate that the dynamics of intraband electron scattering by defects is Markovian (quasistationary) only in the above discussed intermediate interval (ii) in which both the decay and phase variation of a quasiparticle can be expressed in terms of rate constants. Outside this range, i.e., in earlier and later intervals, the decay and/or phase variations of excited quasiparticle wave functions are more complex and cannot be described by simple rates. We have found that for quasiparticle excitation energies $E_{\mathbf{K}} \geq 50$ meV the duration of the intermediate interval, which can be identified with the lifespan of a standard quasiparticle behavior, exceeds ~ 850 fs and grows longer as $E_{\mathbf{K}}$ is in-

creased. The formalisms employed in obtaining these results enabled us to treat electron scattering from random arrays of adsorbates of variable surface density and thereby explore the effects of adsorbate concentration on the quasiparticle dynamics. In Secs. III and IV we found that in the studied system the quasiparticle evolution is dominated by the effects that are linear in concentration of random scatterers up to $c \sim 7\%$, which amply covers the situations studied experimentally.^{17,18}

Electron spectroscopy measurements of the electronic structure of gaseous and condensed matter involve in one way or another the injection or removal of quasiparticles (electrons or holes) into or from the states of the studied system. These are highly nonadiabatic processes and descriptions of quasiparticle propagation in the initial, intermediate, or final states of the probed systems should therefore involve propagators of the form described by Eq. (6) if the scattering from defects may have strong impact on quasiparticle dynamics. Analogous situation occurs in the studies of quasiparticle dynamics affected by the interactions with other types of excitations (i.e., the dynamical degrees of freedom) in the system.^{38,39} Hence, it is of general importance for spectroscopic measurements to understand all the aspects of quasiparticle dynamics on both the ultrafast and asymptotic time scales. This particularly refers to simple modelings of the dynamics of multiply excited systems because the validity of such descriptions may be restricted by the time scale(s) of the various relaxation processes. Typical examples are the modelings of 2PPE yields from bulk and surface bands of solids in pump-probe experiments by optical Bloch equations which in their standard form apply only to the studies of relaxation processes in the Markovian regime. However, as the present and recent^{38,39,42} studies of quasiparticle dynamics in surface bands demonstrate strong deviations of quasiparticle relaxations from the Markovian limit, particularly for the quasiparticle states close to the respective band bottoms, great care should be taken in assessing the results of applications of such phenomenological models to describe the system response on ultrashort time scales. One of the goals of the present study was to elucidate these aspects of ultrafast electron dynamics on the example of ubiquitous type of interactions in surface bands.

So far 2PPE experiments have been interpreted successfully using exponential decay as given by Fermi’s golden rule. The initial quadratic decay occurs on time scales at the lower end of the range which is available experimentally (~ 10 fs) at photon energies in the visible or ultraviolet. With recent advances in attosecond spectroscopy⁶⁴ the Zeno decay regime might be accessible in the near future. Its observation and crossover to a different decay regime may be additionally facilitated by the variation of characteristic decay times with adsorbate concentration [$\tau_Z \propto 1/\sqrt{c}$ and $\tau_{\mathbf{K}}^{\text{sc}} \propto 1/c$, cf. Fig. 16 and discussions following expressions (23) and (27)], which according to our findings persist in a sufficiently large interval of c values.

The collapse of the initial-state survival probability occurs at propagation times easily accessible in experiments. However, the survival probability beyond collapse is extremely small, so it would be hard to detect even in the best experiments covering currently more than 5 orders of magnitude

dynamical range. An exception is the case $K=0$ (see Fig. 8), however, there is no experimental evidence for a slower decay rate¹⁵ or decreased intraband scattering rate near the band bottom.¹⁷ A possible explanation could be that the lost quasiparticle identity is restored in the second photoemission step leading to the emission of an electron.

Elastic intraband scattering as considered here leads only to a change in the momentum of the IS electron within the same band.¹⁸ Therefore dephasing is usually observed in the spectral rather than in the time domain. The deviation from the FGR decay arises from the poles near the band bottom of the spectra (see Figs. 5–7). However, the spectral weight in that region is rather small to be detected in a line shape analysis. An exception occurs again for the case $K=0$. The shift of the spectral weight with energy $E_{\mathbf{k}}$ should influence the dispersion and lead to a coverage-dependent effective mass. The Zeno decay regime would be observable for energies far away from the main peak. The line shape analysis would require an extremely careful spectral characterization of the laser pulses and the transmission function of the energy analyzer. An additional difficulty arises, because the

spectral linewidth changes considerably with delay time for small delays.³⁵

It would be interesting to extend the current model to more than one band. This would open the possibility to describe elastic interband scattering¹⁵ or dephasing in quantum beats patterns.^{11,65}

The main purpose of this work was to explore the time range of exponential decay for elastic electron scattering by random adsorbates, viz. the lifespan of standard quasiparticle behavior. Three different methods were employed and they yielded similar results. The observation of the deviation from exponential decay currently remains an experimental challenge.

ACKNOWLEDGMENTS

This work was supported in part by the Ministry of Science, Education and Sports of Republic of Croatia through Research Project Nos. 035-0352828-2839, 035-0352828-2837, and 119-0000000-1015.

-
- ¹R. Haight, Surf. Sci. Rep. **21**, 275 (1995).
²E. Bertel, Surf. Sci. **331-333**, 1136 (1995).
³Th. Fauster and W. Steinmann, in *Electromagnetic Waves: Recent Developments in Research*, edited by P. Halevi (North Holland, Amsterdam, 1995), Vol. 2, p. 347.
⁴T. Hertel, E. Knoesel, M. Wolf, and G. Ertl, Phys. Rev. Lett. **76**, 535 (1996).
⁵M. Wolf, E. Knoesel, and T. Hertel, Phys. Rev. B **54**, R5295 (1996).
⁶M. Wolf, Surf. Sci. **377-379**, 343 (1997).
⁷M. Wolf, A. Hotzel, E. Knoesel, and D. Velic, Phys. Rev. B **59**, 5926 (1999).
⁸S. Ogawa, H. Nagano, H. Petek, and A. P. Heberle, Phys. Rev. Lett. **78**, 1339 (1997).
⁹H. Petek, A. P. Heberle, W. Nessler, H. Nagano, S. Kubota, S. Matsunami, N. Moriya, and S. Ogawa, Phys. Rev. Lett. **79**, 4649 (1997).
¹⁰H. Petek and S. Ogawa, Prog. Surf. Sci. **56**, 239 (1997).
¹¹U. Höfer, I. L. Shumay, Ch. Reuß, U. Thomann, W. Wallauer, and Th. Fauster, Science **277**, 1480 (1997).
¹²C. Reuß, I. L. Shumay, U. Thomann, M. Kutschera, M. Weinelt, T. Fauster, and U. Höfer, Phys. Rev. Lett. **82**, 153 (1999).
¹³M. Weinelt, J. Phys.: Condens. Matter **14**, R1099 (2002).
¹⁴T. Hertel, E. Knoesel, E. Hasselbrink, M. Wolf, and G. Ertl, Surf. Sci. **317**, L1147 (1994).
¹⁵K. Boger, M. Weinelt, and Th. Fauster, Phys. Rev. Lett. **92**, 126803 (2004).
¹⁶K. Boger, M. Weinelt, J. Wang, and Th. Fauster, Appl. Phys. A: Mater. Sci. Process. **78**, 161 (2004).
¹⁷K. Boger, Th. Fauster, and M. Weinelt, New J. Phys. **7**, 110 (2005).
¹⁸Th. Fauster, M. Weinelt, and U. Höfer, Prog. Surf. Sci. **82**, 224 (2007).
¹⁹S. Smadici and R. M. Osgood, Phys. Rev. B **71**, 165424 (2005).
²⁰P. M. Echenique, J. M. Pitarke, E. V. Chulkov, and A. Rubio, Chem. Phys. **251**, 1 (2000).
²¹P. M. Echenique, R. Berndt, E. V. Chulkov, Th. Fauster, A. Goldman, and U. Höfer, Surf. Sci. Rep. **52**, 219 (2004).
²²E. V. Chulkov, A. G. Borisov, J. P. Gauyacq, D. Sánchez-Portal, V. M. Silkin, V. P. Zhukov, and P. M. Echenique, Chem. Rev. (Washington, D.C.) **106**, 4160 (2006).
²³H. Ueba, Surf. Sci. **334**, L719 (1995).
²⁴M. Sakaue, T. Munakata, H. Kasai, and A. Okiji, Phys. Rev. B **66**, 094302 (2002); **68**, 205421 (2003); Surf. Sci. **532-535**, 30 (2003).
²⁵M. Sakaue, J. Phys.: Condens. Matter **17**, S245 (2005).
²⁶H. Ueba and B. Gumhalter, Prog. Surf. Sci. **82**, 193 (2007).
²⁷A. G. Borisov, A. K. Kazansky, and J. P. Gauyacq, Phys. Rev. B **65**, 205414 (2002).
²⁸A. G. Borisov, J. P. Gauyacq, and A. K. Kazansky, Surf. Sci. **540**, 407 (2003).
²⁹J. P. Gauyacq, A. G. Borisov, and A. K. Kazansky, Appl. Phys. A: Mater. Sci. Process. **78**, 141 (2004).
³⁰F. E. Olsson, M. Persson, A. G. Borisov, J. P. Gauyacq, J. Lagoute, and S. Fölsch, Phys. Rev. Lett. **93**, 206803 (2004).
³¹F. E. Olsson, A. G. Borisov, M. Persson, N. Lorente, A. K. Kazansky, and J. P. Gauyacq, Phys. Rev. B **70**, 205417 (2004).
³²F. E. Olsson, A. G. Borisov, and J. P. Gauyacq, Surf. Sci. **600**, 2184 (2006).
³³A. K. Kazansky, V. M. Silkin, E. V. Chulkov, A. G. Borisov, and J. P. Gauyacq, Phys. Rev. B **75**, 235412 (2007).
³⁴C. Timm and K. H. Bennemann, J. Phys.: Condens. Matter **16**, 661 (2004).
³⁵K. Boger, M. Roth, M. Weinelt, Th. Fauster, and P.-G. Reinhard, Phys. Rev. B **65**, 075104 (2002).
³⁶J. P. Gauyacq and A. K. Kazansky, Appl. Phys. A: Mater. Sci. Process. **89**, 517 (2007).
³⁷Y. J. Dappe, A. A. Villaeys, and F. P. Lohner, Appl. Surf. Sci.

- 168**, 41 (2000); A. A. Villaeys, Y. J. Dappe, and F. P. Lohner, Phys. Rev. B **63**, 155113 (2001); Y. J. Dappe and A. A. Villaeys, *ibid.* **67**, 235415 (2003).
- ³⁸P. Lazić, V. M. Silkin, E. V. Chulkov, P. M. Echenique, and B. Gumhalter, Phys. Rev. Lett. **97**, 086801 (2006).
- ³⁹P. Lazić, V. M. Silkin, E. V. Chulkov, P. M. Echenique, and B. Gumhalter, Phys. Rev. B **76**, 045420 (2007).
- ⁴⁰B. Gumhalter and H. Petek, Surf. Sci. **445**, 195 (2000).
- ⁴¹B. Gumhalter, Surf. Sci. **518**, 81 (2002).
- ⁴²F. El-Shaer and B. Gumhalter, Phys. Rev. Lett. **93**, 236804 (2004).
- ⁴³B. Gumhalter, Phys. Rev. B **72**, 165406 (2005).
- ⁴⁴V. M. Silkin, J. M. Pitarke, E. V. Chulkov, and P. M. Echenique, Phys. Rev. B **72**, 115435 (2005).
- ⁴⁵J. Gütde, M. Rohleder, T. Meier, S. W. Koch, and U. Höfer, Science **318**, 1287 (2007).
- ⁴⁶N. V. Dobrodey, L. S. Cederbaum, and F. Tarantelli, Phys. Rev. B **57**, 7340 (1998).
- ⁴⁷S. Doniach and E. H. Sondheimer, *Green's Functions for Solid State Physicists* (Benjamin, Reading, MA, 1974), Chap. 5.
- ⁴⁸The principle of particle *injection* into empty states of a system implies temporal boundary conditions in which the particle interactions with the system are switched on nonadiabatically. Besides the use of this principle in specific theoretical formulations of electron dynamics in terms of quasiparticle propagators (Ref. 47), it has also been employed in the interpretations of 2PPE experiments from surface bands (Ref. 66) and of hyperthermal molecular desorption from surfaces (Ref. 67). The opposite case of adiabatic switching on of particle interactions with the system is more appropriate to the formulations of surface scattering theory, be the interactions treated quantum-mechanically (Ref. 68) or semiclassically (Ref. 69).
- ⁴⁹E. Ruffeil Fiori and H. M. Pastawski, Chem. Phys. Lett. **420**, 35 (2006); Braz. J. Phys. **36**, 844 (2006).
- ⁵⁰The interband matrix elements of the dipole potential are in the relevant range of momentum transfer almost 1 order of magnitude weaker than the intraband ones.
- ⁵¹B. Simon, Ann. Phys. (N.Y.) **97**, 279 (1976).
- ⁵²V. Madhavan, W. Chen, T. Jamneala, M. F. Crommie, and N. S. Wingreen, Phys. Rev. B **64**, 165412 (2001); L. Bartels, S. W. Hla, A. Kühnle, G. Meyer, K.-H. Rieder, and J. R. Manson, *ibid.* **67**, 205416 (2003); E. Dupont-Ferrier, P. Mallet, L. Magaud, and J. Y. Veuillen, Europhys. Lett. **72**, 430 (2005); L. Limot, E. Pehlke, J. Kröger, and R. Berndt, Phys. Rev. Lett. **94**, 036805 (2005).
- ⁵³P. Facchi, H. Nakazato, and S. Pascazio, Phys. Rev. Lett. **86**, 2699 (2001).
- ⁵⁴P. Facchi and S. Pascazio, Phys. Lett. A **241**, 139 (1998).
- ⁵⁵P. Facchi and S. Pascazio, Physica A **271**, 133 (1999).
- ⁵⁶L. Khalfin, Sov. Phys. JETP **6**, 1053 (1958).
- ⁵⁷L. Fonda, G. C. Ghirardi, and A. Rimini, Rep. Prog. Phys. **41**, 587 (1978).
- ⁵⁸A. Peres, Ann. Phys. (N.Y.) **129**, 33 (1980).
- ⁵⁹A. K. Kazansky, J. Phys. B **30**, 1401 (1997).
- ⁶⁰We acknowledge useful discussions on this issue with Prof. J. Tambača.
- ⁶¹B. Kramer, A. MacKinnon, and D. Weaire, Phys. Rev. B **23**, 6357 (1981).
- ⁶²A. Šiber, Am. J. Phys. **74**, 692 (2006).
- ⁶³J. L. Richardson, Comput. Phys. Commun. **63**, 84 (1991).
- ⁶⁴A. L. Cavalieri, N. Müller, Th. Uphues, V. S. Yakovlev, A. Baltuška, B. Horvath, B. Schmidt, L. Blümel, R. Holzwarth, S. Hendel, M. Drescher, U. Kleineberg, P. M. Echenique, R. Kienberger, F. Krausz, and U. Heinzmann, Nature (London) **449**, 1029 (2007).
- ⁶⁵M. Hirschmann and Th. Fauster, Appl. Phys. A: Mater. Sci. Process. **88**, 547 (2007).
- ⁶⁶A. Winkelmann, F. Bisio, R. Ocaña, W.-C. Lin, M. Nývlt, H. Petek, and J. Kirschner, Phys. Rev. Lett. **98**, 226601 (2007).
- ⁶⁷B. Gumhalter and T. Matsushima, Surf. Sci. **561**, 183 (2004).
- ⁶⁸B. Gumhalter, Phys. Rep. **351**, 1 (2001).
- ⁶⁹A. Bilić, B. Gumhalter, W. Mix, A. Golichowski, S. Tzanev, and K. J. Snowdon, Surf. Sci. **307-309**, 165 (1994); A. Bilić, B. Gumhalter, and K. J. Snowdon, *ibid.* **368**, 71 (1996).